Topological phase transition measured in a dissipative metamaterial

Eric I. Rosenthal, Nicole K. Ehrlich, Mark S. Rudner, Andrew P. Higginbotham, and K. W. Lehnert

Topological phase transition measured in a dissipative metamaterial

Eric I. Rosenthal,[1, 2, *] Nicole K. Ehrlich,[1, 2] Mark S. Rudner,[3] Andrew P. Higginbotham,[1, 2, †] and K. W. Lehnert[1, 2]

[1] *JILA, National Institute of Standards and Technology and the University of Colorado, Boulder, Colorado 80309, USA*
[2] *Department of Physics, University of Colorado, Boulder, Colorado 80309, USA*
[3] *Niels Bohr International Academy and Center for Quantum Devices,*
University of Copenhagen, 2100 Copenhagen, Denmark
(Dated: May 15, 2018)

We construct a metamaterial from radio-frequency harmonic oscillators, and find two topologically distinct phases resulting from dissipation engineered into the system. These phases are distinguished by a quantized value of bulk energy transport. The impulse response of our circuit is measured and used to reconstruct the band structure and winding number of circuit eigenfunctions around a dark mode. Our results demonstrate that dissipative topological transport can occur in a wider class of physical systems than considered before.

When a wave propagates through a periodic medium, its properties can be modified dramatically compared to those in free space. In particular, such "Bloch waves" may exhibit topological effects: robust behaviors that are insensitive to small changes to the medium. In solid state systems, the topological characteristics of electronic Bloch waves are responsible for robustly quantized transport in the integer quantum Hall effect[1,2], and the novel characteristics of topological insulators and superconductors[3–8]. Importantly, many bosonic and even classical systems, such as cold atoms in optical lattices[9,10], as well as photonic[11–19] and mechanical metamaterials[20–23], can also support waves classified by topological invariants.

Remarkably, the presence of loss and/or gain can give rise to qualitatively new topological invariants and phenomena[24–31]. The topological classification of such non-Hermitian systems is different from that of their lossless, Hermitian counterparts. In particular, Ref. 24 studied a non-Hermitian quantum problem, and showed that dissipation (particle loss) can lead to a wholly new type of topologically protected quantized transport, which has no analogue in particle conserving systems. Specifically, the mean displacement achieved by a particle between its initialization and decay changes sharply between two quantized values as the relative strengths of the system's two coupling parameters are tuned.

Is this phenomenon specific to first-order-in-time systems governed by an effective non-Hermitian Schrödinger equation (e.g., Refs. 24, 26, and 27)? Or, is this behavior part of a much more general phenomenology of quantized transport in dissipative wave systems? While it is natural, for example, to construct second-order (harmonic) systems with similar eigenmode winding properties to first-order systems, it is nontrivial that *quantized transport* – which generally depends on both the eigenmode wave functions and the dispersion relation – could persist in the harmonic case as well.

In this Rapid Communication, we expose the generality of dissipative topological transport by demonstrating its existence in an electromagnetic circuit (Fig. 1a) governed by *harmonic* (non-Schrödinger-like) equations

of motion. From the impulse response of the circuit we extract the full spatial distribution of dissipated energy. We find that the mean displacement between the location where an energy pulse is injected and where it dissipates takes just one or the other of two quantized values, dependent on the ratio of two coupling parameters (inductances) in the circuit. Through analytical arguments and numerical simulations we demonstrate that this transition is *topological*, with quantization becoming exact for an ideal realization of the circuit. The impulse response also yields the circuit's eigenmode profiles, which we use to directly image the topological winding characteristic in wave number space that signifies the transition. Our observation of quantized transport in a classical harmonic system opens the way to exploring topological dynamics in a much wider range of physical systems than considered before.

Circuit model.— We investigate a one-dimensional metamaterial with the unit cell defined in Fig. 1a. Each unit cell, m, is comprised of a lossless 'A-site' with a capacitor c connected to ground, and a lossy 'B-site' with a capacitor c and a resistor r connected in parallel to ground. These circuit nodes are connected by tunable coupling inductors l_A and l_B.

To study energy transport in both simulation and experiment, we initialize a voltage pulse v_0 on one A-site, indexed to be $m_0 = 0$, and measure the impulse response of the circuit by obtaining the time-dependent voltages v_m^A and v_m^B on all A-sites and B-sites, respectively. The initial pulse contains an energy $\frac{1}{2}cv_0^2$. We extract the fraction P_m of this total energy dissipated in each unit cell m; the energy displacement δ, characterizing the asymmetric propagation of energy in the circuit, is defined as the mean of the probability distribution, $\{P_m\}$:

$$\delta = \sum_m (m - m_0) P_m, \quad P_m = \frac{2}{rc} \int_0^\infty dt \left(\frac{v_m^B}{v_0} \right)^2. \quad (1)$$

The limiting behavior of δ is easily understood. When l_B approaches infinity while $l_A \ll l_B$ remains finite, a pulse initialized on the lossless A-site in unit cell m will dissipate only on the right-adjacent B-site, in unit cell $(m + 1)$. This yields $\delta = 1$. When l_A approaches infinity
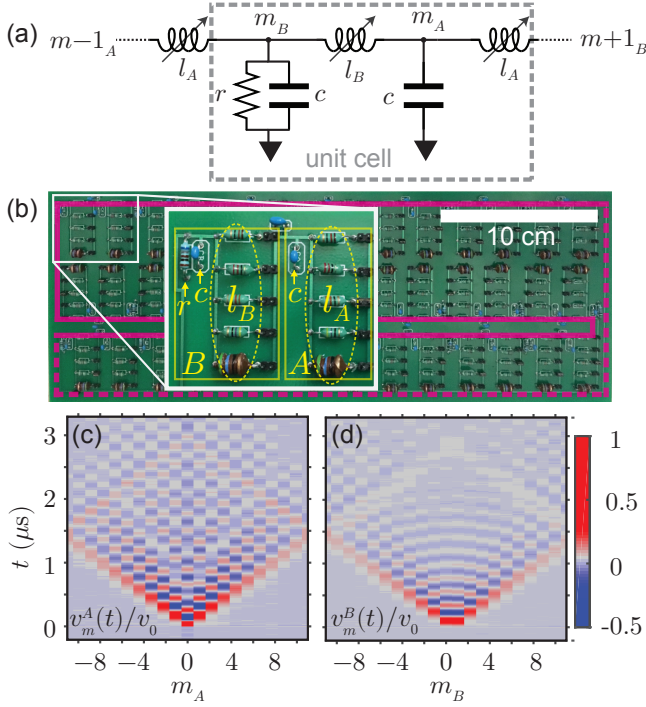
FIG. 1. (a) A topological metamaterial: circuit nodes, indexed by an integer m, are connected to ground with capacitors c, and coupled to each other by variable inductors l_A and l_B. B-sites contain a resistor r to ground, while A-sites do not. (b) Circuit photograph. The inset shows one A-site and one B-site. Coupling inductances are variable by greater than a factor of ten using switch networks. The solid pink line traces a chain of adjacent cells, and the dashed pink line connects the edges of this chain to form periodic boundary conditions. This asymmetric connection has a negligible effect on circuit dynamics; its parasitic capacitance is calculated to be about 3% of the on-site capacitance, and its length (49 cm) is less than about 1% of the wavelength of light at frequencies of interest. (c,d) The time-dependent voltages measured on A and B sites, $v_m^A(t)$ and $v_m^B(t)$, respectively, are plotted as a function of site index m and time t for the case where $l_A = l_B$. Waveforms are normalized to the voltage v_0, present at site $m_A = 0$ at time $t = 0$.

while $l_B \ll l_A$ remains finite, the pulse will dissipate only on the left-adjacent B-site, within the same unit cell, m. This gives $\delta = 0$. Finally, when $l_A = l_B$, the symmetry of the circuit dictates that an excitation will propagate equally to the left and right, so one may expect $\delta = 1/2$ in this case.

Remarkably, δ does not smoothly transition between these limiting cases, but rather remains integer-valued as long as $l_A \neq l_B$. To show this, we derive[32] the equations of motion for this circuit using Kirchhoff's circuit laws. In reciprocal space, indexed by the dimensionless wave number $-\pi \leq k < \pi$, dynamics are described in terms of the (complex) variables $v_k^{A(B)}(t) = \sum_m e^{-ikm} v_m^{A(B)}(t)$. The circuit equations of motion break into a collection of
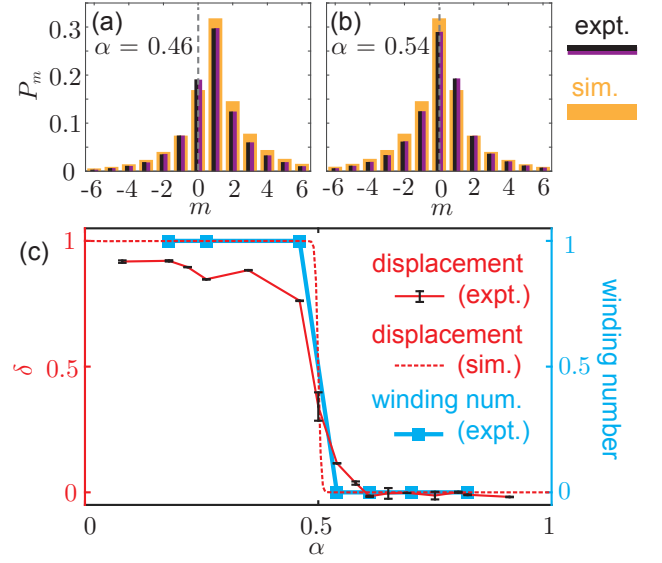

FIG. 2. Fraction of the total energy dissipated, P_m vs. m, for (a) the topological phase and (b) the trivial phase of our circuit. Gray dashed lines indicate $m = 0$, where an excitation is initialized. Two experimental data sets (black and purple distributions) are compared to simulated distributions (orange) of an 'ideal' circuit with no disorder, no additional loss, and 501 unit cells. (c) Mean displacement δ as a function of $\alpha = l_A/(l_B + l_A)$ for the mean of both experimental data sets (solid red line) and a numerical simulation (dashed red line) of an ideal circuit. Black lines show the range of δ over both experimental runs, which is nearly zero for most values of α. A phase transition between $\delta = 1$ and $\delta = 0$ occurs around $\alpha = 0.5$. The behavior of δ approximates the winding number of $\xi_{j,k}$ around the dark state (blue line).

2×2 linear systems, associated with each value of k:

$$\begin{pmatrix} \omega_0^2 + \partial_t^2 & g_k \\ g_k^* & \omega_0^2 + \gamma\partial_t + \partial_t^2 \end{pmatrix} \begin{pmatrix} v_k^A \\ v_k^B \end{pmatrix} = 0. \qquad (2)$$

For each k, Eq. (2) describes two coupled harmonic oscillators, one of which is damped. The system is parametrized by a resonance frequency $\omega_0 = \sqrt{(l_A + l_B)/(l_A l_B c)}$, a loss rate $\gamma = 1/(rc)$, and a complex coupling $g_k = -\omega_0^2 (\alpha + \beta e^{ik})$ between the A and B sublattice oscillators. Here $\alpha = l_A/(l_A + l_B)$ and $\beta = l_B/(l_A + l_B) = 1 - \alpha$.

When $\alpha = 1/2$, the coupling parameter $g_{k=\pi}$ becomes zero and the sublattices completely decouple. At this special point in parameter space the system possesses a "dark state:" an excitation on the A sublattice with $k = \pi$ is decoupled from any source of loss and therefore acquires an infinite lifetime[33]. Analogous to the situation in non-Hermitian quantum systems[24], for $\alpha \neq 1/2$ the Bloch eigenfunctions can be classified by a topological winding number that counts the number of times the relative phase of the A and B components runs through 2π as k traverses the Brillouin zone.

Closely related to this winding number, Eqs. (1) and (2) predict[32] the displacement δ to be quantized as a function of α:

$$\delta = \oint \frac{dk}{2\pi} \frac{\partial \theta_k}{\partial k} = \begin{cases} 1 & \text{if } \alpha < 1/2 \\ 0 & \text{if } \alpha > 1/2 \end{cases}, \tag{3}$$

where $\theta_k = \arg\{g_k\}$ is the k-dependent angle of g_k in the complex plane.

Time-domain numerical simulations using a Runge-Kutta method[34,35] of a system with 501 unit cells and periodic boundary conditions closely match the analytic result of Eq. (3). Histograms of the spatial distribution of P_m in the simulation are shown in Fig. 2a and Fig. 2b for $\alpha = 0.46$ and $\alpha = 0.54$, respectively. This distribution is computed for many different values of α and is centered around $m = 1$ when $\alpha < 0.5$, and $m = 0$ when $\alpha > 0.5$. Thus the plot of the simulated δ vs. α in Fig. 2c displays the step-function behavior predicted by Eq. (3).

Experimental measurements.— We test the robustness of our theoretical results to real-world imperfections and perturbations with an experiment on a circuit of 21 unit cells and periodic boundary conditions (Fig. 1b). In the circuit we use capacitors with $c = 381.5\,\text{pF}$, resistors with $r = 681\,\Omega$, and coupling inductors with inductances l_A and l_B that can each be set between $5.3\,\mu\text{H}$ and $56.7\,\mu\text{H}$. We probe the circuit dynamics by applying a voltage impulse v_0 to one A-site and measuring the subsequent voltage as a function of time on all circuit nodes using an oscilloscope (Fig. S1).

Examples of A-site and B-site waveforms are plotted in Fig. 1c and Fig. 1d, respectively, for the special case when $l_A = l_B$. The longer-lived anti-phase excitations which occur predominantly on the A-sublattice are characteristic of the dark state present in this symmetric configuration[36]. Any anti-phase excitations on the B-sublattice are heavily damped due to maximum possible coupling to the resistors, the circuit's dominant source of loss. The displacement δ is calculated from the B-site waveforms measured when the circuit has been tuned to different values of α (see, e.g., Fig. 1d for $\alpha = 0.5$).

Although a phase transition is qualitatively apparent in experiment, it is not as sharp as the step function predicted by theory (Eq. 3) and simulation (Fig. 2c). Sharpness is reduced by undesired loss, disorder and a finite lattice size (Fig. S3). A significant source of undesired loss in our experiment is the resistive losses of the coupling inductors, which is between 4 and 29 Ω (Table S1), compared to their reactive impedance of between 0.3 kΩ to 1.4 kΩ, respectively, at 4 MHz.

The most striking deviation of our experiment from theory is that the measurements of δ do not quite approach a value of one as α goes to zero. The finite size of our system combined with periodic boundary conditions contributes to this effect: even at our lowest attainable value of α, the impedance of the coupling inductors is small enough to allow some fraction of the initial excitation to propagate more than halfway around the circuit.

Such excursions can significantly alter the obtained value of the mean displacement (Fig. S3).

To explore the underlying topological nature of the transition observed in Fig. 2c, we experimentally reconstruct the circuit's band structure and eigenvectors. The impulse response of our circuit encodes all eigenvectors of the family of equations described by Eq. (2), which are all excited simultaneously. We analyze this response by Fourier transforming the measured waveforms (e.g., Figs. 1c,d) in *both* spatial index and time, in order to obtain the circuit's band structure. The Fourier transform is defined as $v_k^{A(B)}(\omega) = \sum_{t,m} e^{-i(\omega t + km)} v_m^{A(B)}(t)$, where $v_k^A(\omega)$ and $v_k^B(\omega)$ are the complex valued Fourier domain voltages on the A and B sublattices, and t is a discrete time variable with $t = 2\,\text{ns} \times \{1, 2 \ldots 2500\}$.

In Figs. 3a, 3b and 3c we show $|v_k^A(\omega)|$ for $\alpha < 0.5$, $\alpha = 0.5$ and $\alpha > 0.5$, respectively. In all cases, we observe two bands with frequencies that agree closely with the dispersion relation calculated from Eq. (2) (white dashed lines). Note that in the absence of loss, the circuit features a light-like linear dispersion relation at long wavelengths, in contrast to the particle-like quadractic dispersion of the non-Hermitian systems previously shown to exhibit quantized transport[24,26].

The complex values of $v_k^A(\omega)$ at its intensity peaks encode the A-sublattice components of the corresponding Bloch eigenvectors, $V_{j,k}^A$, where $j = 1, 2$ is a band index labeling the lower and upper bands, respectively. We extract the values of $V_{j,k}^A$ by taking a vertical linecut of the A-sublattice band structure (Fig. 3a–c) at each value of k, and returning the values of $v_k^A(\omega)$ at the two local maxima of each linecut. The corresponding B-sublattice component of the eigenvector $V_{j,k}^B$ is the set of points on linecuts across the B-sublattice bands (not shown).

The A and B eigenvector components can be parameterized by the following k-dependent complex ratio:

$$\xi_{j,k} = V_{j,k}^B / V_{j,k}^A. \tag{4}$$

For most values of k and α we see $|\xi_{j,k}| \approx 1$, indicating that the eigenmodes are equally distributed on the two sublattices. However near the dark state, i.e., for $\alpha \approx 0.5$ and $k \approx \pi$, $|\xi_{j,k}|$ approaches zero and excitations living primarily on the A-sublattice gain long lifetimes (seen by the heavily weighted pixels at $k = \pi$ in Fig. 3b).

Crucially, the k-dependent phase relationship between $V_{j,k}^A$ and $V_{j,k}^B$ distinguishes the two topologically distinct phases of the system. Due to the continuity and periodicity of $V_{j,k}^A$ and $V_{j,k}^B$ in the Brillouin zone, $\xi_{j,k}$ forms a closed loop in the complex plane. As long as $0 < |\xi_{j,k}| < \infty$, such loops can be classified by the integer number of times that $\xi_{j,k}$ winds around the origin as k goes from 0 to 2π. Thus the topological invariant of our circuit is simply the winding number of $\xi_{j,k}$ around the origin of the complex plane, or, equivalently, around the dark state in parameter space.

From the experimental data we reconstruct $\xi_{j,k}$ (Figs. 3d–f). These plots clearly show the winding number transition from 1 to 0 as α is changed from 0.26
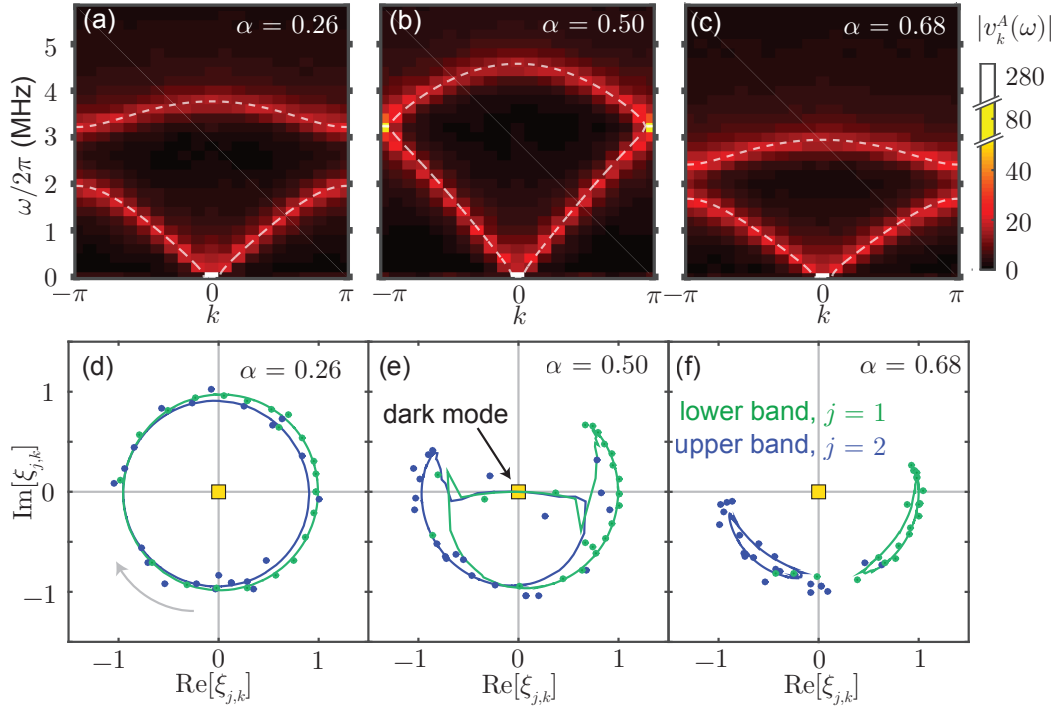
FIG. 3. (a,b,c) Circuit band structure, exhibited in the Fourier-transformed A-sublattice voltages, $|v_k^A(\omega)|$. A dark mode appears at $\alpha = l_A/(l_A + l_B) = 0.5$ and $k = \pi$. The dashed white lines show the real parts of the circuit's complex eigenfrequencies, found by diagonalizing Eq. (2) with the same circuit parameter values that are used in each experiment. Eigenvector sublattice components $V_{j,k}^A$ and $V_{j,k}^B$ are extracted from linecuts across the lower ($j = 1$) and upper ($j = 2$) bands. (d,e,f) The complex ratio $\xi_{j,k} = V_{j,k}^B/V_{j,k}^A$, whose winding number around the origin (the location of the dark mode, yellow square) distinguishes the topological phases of the circuit. Experimental points (dots) agree closely with results of a numerical simulation (lines).

to 0.68. These two phases are separated by the case of $\alpha = 0.5$ where $\xi_{j,k}$ intersects the origin and its winding number is undefined. This behavior of the winding number as a function of α is closely approximated by the measured behavior of δ, see Fig. 2c.

Unlike many other topological transitions in periodic systems, the transition in our circuit is not associated with the closing of gap in the band structure. Rather, the transition is characterized by a vanishing of the *imaginary* part of one of the system's eigenvalues. In particular, the transition persists in a circuit where the A-site and B-site capacitors are unequal, so that the bandgap does not close for any value of α (Fig. S4).

Discussion.— Our observations suggest that dissipative quantized transport may be realized in a much wider class of dynamical systems than previously expected. Given that high-order linear systems can be reparametrized as first-order systems involving a larger number of variables (bands), it is natural to wonder if the classification for multi-band non-Hermitian quantum

walks developed in Ref. 27 can be applied to the second-order system studied in this work. While the equations of motion for our circuit can be recast as a four-band effective non-Hermitian Schrödinger equation [Eq. (S10)], the physical constraints of the circuit (such as charge conservation) impose a special structure on the resulting Bloch Hamiltonians, which was not accounted for in the arguments of Ref. 27. Elucidating the nature of topological transport in our system, the full range of conditions where it can be realized, and its broader implications (in relation to a general topological classification for dissipative systems[37]) will be interesting directions for future work.

* eric.rosenthal@colorado.edu
† Microsoft Q, Copenhagen, Denmark

[1] K. v. Klitzing, G. Dorda, and M. Pepper, Phys. Rev. Lett. **45**, 494 (1980).

[2] D. J. Thouless, Phys. Rev. B **27**, 6083 (1983).

[3] C. L. Kane and E. J. Mele, Phys. Rev. Lett. **95**, 146802 (2005).

[4] C. L. Kane and E. J. Mele, Phys. Rev. Lett. **95**, 226801 (2005).

[5] X.-L. Qi and S.-C. Zhang, Rev. Mod. Phys. **83**, 1057 (2011).

[6] M. Z. Hasan and C. L. Kane, Rev. Mod. Phys. **82**, 3045 (2010).

[7] B. A. Bernevig, "Topological insulators and topological superconductors," (2013).

[8] C.-K. Chiu, J. C. Y. Teo, A. P. Schnyder, and S. Ryu, Rev. Mod. Phys. **88**, 035005 (2016).

[9] T. D. Stanescu, V. Galitski, J. Y. Vaishnav, C. W. Clark, and S. Das Sarma, Phys. Rev. A **79**, 053639 (2009).

[10] N. Goldman, J. C. Budich, and P. Zoller, Nature Physics **12**, 639 (2016).

[11] M. C. Rechtsman, J. M. Zeuner, Y. Plotnik, Y. Lumer, D. Podolsky, F. Dreisow, S. Nolte, M. Segev, and A. Szameit, Nature **496**, 196 (2013).

[12] L. Lu, J. D. Joannopoulos, and M. Soljačić, Nature photonics **8**, 821829 (2014).

[13] S. Mittal, J. Fan, S. Faez, A. Migdall, J. M. Taylor, and M. Hafezi, Phys. Rev. Lett. **113**, 087403 (2014).

[14] J. Ningyuan, C. Owens, A. Sommer, D. Schuster, and J. Simon, Phys. Rev. X **5**, 021031 (2015).

[15] S. Mittal, S. Ganeshan, J. Fan, A. Vaezi, and M. Hafezi, Nature Photonics **10**, 180 (2016).

[16] B. M. Anderson, R. Ma, C. Owens, D. I. Schuster, and J. Simon, Phys. Rev. X **6**, 041043 (2016).

[17] X. Cheng, C. Jouvaud, X. Ni, S. H. Mousavi, A. Z. Genack, and A. B. Khanikaev, Nature Materials **15**, 542 (2016).

[18] C. Owens, A. LaChapelle, B. Saxberg, B. M. Anderson, R. Ma, J. Simon, and D. I. Schuster, Phys. Rev. A **97**, 013818 (2018).

[19] Y. Hadad, J. C. Soric, A. B. Khanikaev, and A. Alù, Nature Electronics **1**, 178 (2018).

[20] C. L. Kane and T. C. Lubensky, Nature Physics **10**, 39 (2014).

[21] J. Paulose, B. G. Chen, and V. Vitelli, Nature Physics **11**, 153 (2015).

[22] R. Süsstrunk and S. D. Huber, Proceedings of the National Academy of Sciences **113**, E4767 (2016).

[23] S. D. Huber, Nature Physics **12**, 621 (2016).

[24] M. S. Rudner and L. S. Levitov, Phys. Rev. Lett. **102**, 065703 (2009).

[25] S. Diehl, E. Rico, M. A. Baranov, and P. Zoller, Nature Physics **7**, 971 (2011).

[26] J. M. Zeuner, M. C. Rechtsman, Y. Plotnik, Y. Lumer, S. Nolte, M. S. Rudner, M. Segev, and A. Szameit, Phys. Rev. Lett. **115**, 040402 (2015).

[27] M. S. Rudner, M. Levin, and L. S. Levitov, arXiv preprint arXiv:1605.07652 (2016).

[28] D. Leykam, K. Y. Bliokh, C. Huang, Y. D. Chong, and F. Nori, Phys. Rev. Lett. **118**, 040401 (2017).

[29] T. Rakovszky, J. K. Asbóth, and A. Alberti, Phys. Rev. B **95**, 201407 (2017).

[30] X. Zhan, L. Xiao, Z. Bian, K. Wang, X. Qiu, B. C. Sanders, W. Yi, and P. Xue, Phys. Rev. Lett. **119**, 130501 (2017).

[31] S. Weimann, M. Kremer, Y. Plotnik, Y. Lumer, S. Nolte, K. G. Makris, M. Segev, M. C. Rechtsman, and A. Szameitr, Nature Materials **16**, 433438 (2017).

[32] See Supplementary Material at [...] for a derivation.

[33] In direct space, the dark state corresponds to voltages on neighboring A-sites oscillating in anti-phase ($k = \pi$), with zero amplitude on the lossy B-sites.

[34] J. R. Dormand and P. J. Prince, J. Comp. Appl. Math **6**, 19 (1980).

[35] L. F. Shampine and M. W. Reichelt, SIAM Journal on Scientific Computing **18**, 1 (1997).

[36] Note that a finite-size lattice with periodic boundary conditions and an *odd* number of unit cells, N, does not support a true dark state (Fig. S2). In this case, the allowed set of crystal momentum values, $k_n = 2\pi n/N$, where $n = 0, 1, 2, \ldots, N-1$, does not include $k = \pi$. Modes with k values close to π still exhibit long lifetimes, with lifetime increasing when α is near $1/2$ and the number of unit cells increases.

[37] Z. Gong, Y. Ashida, K. Kawabata, K. Takasan, S. Higashikawa, and M. Ueda, arXiv preprint arXiv:1802.07964 (2018).